Chapter 3

Vibrational dynamics, phonon dispersion and specific heat in gas permeable poly(4-methyl-2-pentyne)

3.1 INTRODUCTION

Polyacetylene is the best-known conjugated polymer, but its intractability and instability have greatly limited its scope of practical applications [1]. Attachments of appropriate substituents or pendants to the polyene backbone can improve its processability and stability as well as applications. These substituted PAs with appropriate backbone-pendant combinations show various functional properties such as liquid crystallinity, photoconductivity, light emission, ionic susceptibility, photo resistance, chromism, helical chirality, optical nonlinearity, and gas permeability etc. [2].

The separation of hydrocarbons from permanent gases is of considerable importance in the chemical industry. Due to it's extreme permeability to hydrocarbons and high hydrocarbon/permanent gas selectivity, poly(1-trimethylsilyl-1-propyne)[PTMSP] is studied the most [3]. However, the poor chemical resistance of this material limits its use as a membrane for industrial applications. To overcome this problem, an alternative acetylene-based polymer, poly(4-methyl-2-pentyne) [PMP], which exhibits much better chemical resistance than PTMSP can be used [4]. Although PMP has lower organic-vapor/permanent-gas selectivity and permeability than PTMSP, but, it can be raised by nano-porous, nano-sized, fumed silica fillers in membranes of the polymer [5].

Poly(4-methyl-2-pentyne) (PMP) is among the hydrocarbon disubstituted polyacetylenes which have been synthesized to date [6]. These amorphous glassy polymers show high glass transition temperatures (above 200^{o}C), unique permeability parameters, and good mechanical behavior. This polymer combines excellent gas and vapor permeability with good resistance to organic solvents. The high gas permeabilities in PMP result from its very high free volume, and probably, interconnectivity of the free-volume-elements. PMP offers promise in the manufacture of nanocomposite membranes for the

separation of various hydrocarbon mixtures [7]. It is also of importance as its monomer, 4-methyl-2-pentyne, can be easily derived from commercial compounds, 4-methyl-2-pentene or methyl isobutyl ketone, produced on a large scale.

It is known that PMP exists in cis and trans configurations. Synthetic conditions (i.e. the used catalyst, temperature, solvent), macromolecules of substituted polyacetylenes decides percentage of different configurations (*cis* or *trans*) [8]. In turn, different geometries of macromolecules can influence the supramolecular packing of the polymer, which primarily defines its properties, such as solubility, permeability, sorption, etc. The IR spectra and qualitative assignments of few bands are given in literature [9-10].

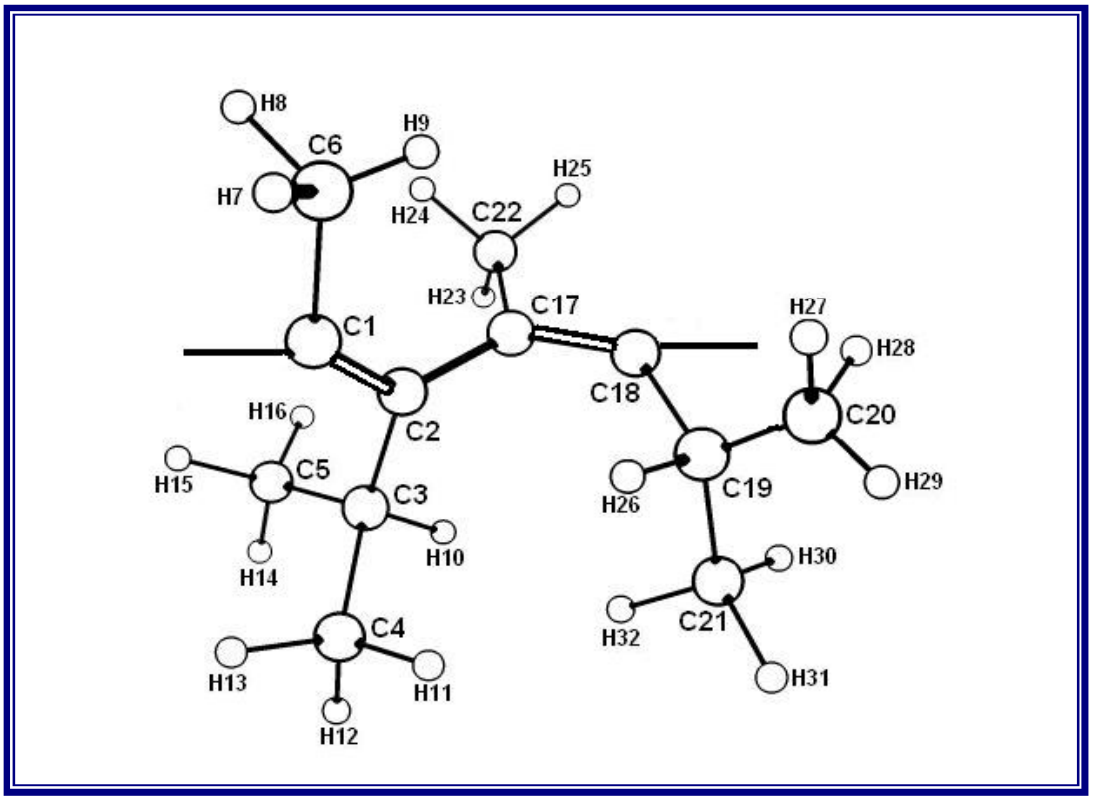

Figure 3.1 Constitutional Repeating Unit of PMP

However, to understand fully the spectroscopic behaviour of PMP, complete quantitative study is desired. Vibrational dynamical studies provide quantitative interpretation of IR and Raman spectra. The dispersion curves enable us to appreciate the origin of the symmetry dependent and symmetry independent spectral features. They can also correlate microscopic properties to macroscopic properties like specific heat etc.

3.2 THEORY

3.2.1 Calculation of normal mode frequencies

Higgs [11] utilized the helical symmetry present in a polymer molecule in order to adapt the Wilson's GF matrix method [12]. The potential interaction and the kinetic coupling between the i^{th} internal coordinate of the n^{th} unit and the k^{th} internal coordinate of the n'^{th} unit are given by the matrix element $F_{ik}^{nn'}$ and $G_{ik}^{nn'}$. Now the periodicity of the chain requires that these matrix elements depend on n and n' only through their differences, that is,

$$F_{ik}^{nn'} = F_{ik}^{s} \qquad \text{....(3.1)}$$

$$G_{ik}^{nn'} = G_{ik}^{s} \qquad \text{….(3.2)}$$

where s = (n-n'). The Wilson's GF matrix method consists of writing the inverse kinetic energy matrix G and potential energy matrix F in internal coordinates R. For infinite isolated helical polymer, there is an infinite number of internal coordinates which lead to G and F matrices of infinite order. Higgs showed that the G and F matrices which are of infinite order can be factored into sets of matrices G(δ) and F(δ) which are of finite order, corresponding to the phase difference δ between the vibration of adjacent units in the chain. The order of G(δ) of F(δ) is equal to N (the number of internal coordinates in a

chemical repeat unit). A Fourier transform on the system of internal displacement coordinate is defined, in order to give a set of internal symmetry coordinates,

$$S(\delta) = \sum_{n=-\infty}^{\infty} R^n \exp(in\delta) \quad \text{....(3.3)}$$

The elements of the G(δ) and F(δ) matrices are then

$$G_{ik} = \sum_{n=-\infty}^{\infty} G_{ik}^s \exp(in\delta) \quad \text{....(3.4)}$$

$$F_{ik} = \sum_{n=-\infty}^{\infty} F_{ik}^s \exp(in\delta) \quad \text{....(3.5)}$$

The secular equation of an infinite order can then be reduced to a set of n^{th} order equations:

$$\left| G(\delta)F(\delta) - \lambda(\delta)I \right| = 0 \quad \text{....(3.6)}$$

Where eigenvalues λ are related with calculated modes. For j^{th} mode the wave number $\tilde{\nu}_j(\delta)$ are given by $\lambda_j(\delta) = 4\pi^2 c^2 \tilde{\nu}_j^2(\delta)$. Here $\tilde{\nu}_j(\delta)$ is expressed in cm^{-1}, c is the velocity of light and $-\pi < \delta < +\pi$. A plot of $\tilde{\nu}_j(\delta)$ versus δ gives the phonon dispersion for the j^{th} mode.

3.2.2 Calculation of Heat Capacity

Dispersion curves can be used to calculate the specific heat capacity of a polymeric system. For a one-dimensional system, the density-of-states function or the frequency distribution function expresses the way energy is distributed among the various branches of normal modes in the crystal and is calculated from the relation:

$$g(\tilde{\nu}) = \sum \left(\partial \tilde{\nu}_j / \partial \delta \right)^{-1} \Big|_{\tilde{\nu}_j(\delta) = \tilde{\nu}_j} \quad \text{....(3.7)}$$

The sum is over all the dispersion branches j. Considering a solid as an assembly of harmonic oscillators, the frequency distribution g ($\tilde{\nu}$) is equivalent to a partition function.

The constant volume heat capacity can be calculated using Debey's relation:

$$C_v = \sum g(\tilde{\nu}_j) k N_A \left(h\tilde{\nu}_j / kT\right)^2 \left[\exp\left(h\tilde{\nu}_j / kT\right) / \left\{\exp\left(h\tilde{\nu}_j / kT\right) - 1\right\}^2\right] \quad \text{....(3.8)}$$

with $\int g(\tilde{\nu}_j) d\tilde{\nu}_j = 1$

TABLE 3.1

Internal coordinates and Urey Bradley force constants (mdyne/Å) for PMP

Internal Coordinates	Force Constants	Internal Coordinates	Force Constants
ν[C1=C2]	7.44	ϕ[C4-C3-H]	0.404(0.200)
ν[C1-C6]	2.46	ϕ[C3-C4-H]	0.357(0.280)
ν[C2-C3]	2.61	ϕ[H-C4-H]	0.388(0.323)
ν[C3-C4]	2.02	ϕ[C1-C6-H]	0.346(0.280)
ν[C3-H]	4.39	ϕ[H-C6-H]	0.392(0.323)
ν[C4-H]	4.09	ϕ[C2-C17-C18]	0.240(0.500)
ν[C6-H]	4.09	ϕ[C2-C17-C22]	0.420(0.175)
ν[C2-C17]	1.76	ϕ[C18-C17-C22]	0.418(0.172)
ϕ[C1-C2-C3]	0.380(0.172)	τ[C2-C3]	0.025
ϕ[C1-C2-C17]	0.260(0.500)	τ[C3-C4]	0.010
ϕ[C3-C2-C17]	0.384(0.170)	τ[C2-C17]	0.018
ϕ[C2-C3-C4]	0.475(0.175)	τ[C17-C18]	0.280
ϕ[C2-C3-H]	0.585(0.230)	τ[C17-C22]	0.010
ϕ[C4-C3-C5]	0.405(0.175)		

Note: 1. ν, ϕ, ω and τ denote stretch, angle bend, wag and torsion, respectively.
2. Non-bonded interactions are given in parentheses.

3.3 RESULTS AND DISCUSSION

The chemical repeat unit of PMP is shown in Fig. 3.1. It contains 32 atoms giving rise to 96 dispersion curves. The frequencies have been calculated for the values $\delta=0$ to $\delta=\pi$ in steps of 0.05π. Due to lacking of conjugation [9], the geometrical parameters are set so that all four carbon atoms at the double bond of the repeating unit were situated in one plane and the double bonds of neighboring units were moved out from this plane by 90^{o}. Geometrical parameters are obtained by energy minimization for a long chain using SPARTAN'02 and HYPERCHEM 7.5.

In the present work, we used the Urey-Bradley force field (UBFF) [13], as it is more comprehensive than the valence force field. UBFF is transferable from same environment, require relatively fewer parameters to express the potential energy, no quadratic terms, cross terms are included, the interaction between non-bonded atoms in gem and tetra-configuration can be included and the arbitrariness in choosing the force constant is reduced. Force constants have been calculated by the least square fitting. Force constants were initially transferred from polyacetylene [PA] [14] and poly(4-methyl-1pentene) [15] and then modified to best fit (modified force constants are given in Table 3.1) to the observed vibrational modes. The assignments are based on potential energy distribution (PED), line intensity, line profile and groups placed in similar environment. Trans rich PMP was synthesized using the catalysts, niobium pentachloride ($NbC1_5$) and triphenyl bismuth (Ph_3Bi), by Marisato et al. [10]. IR spectra (Fig. 3.2) has been used with permission.

Due to availability of spectra only up to 450 cm^{-1}, the assignments below this region could not be precisely made. However, since the calculated frequencies in the higher region where they are in good agreement with the observed ones depend on both

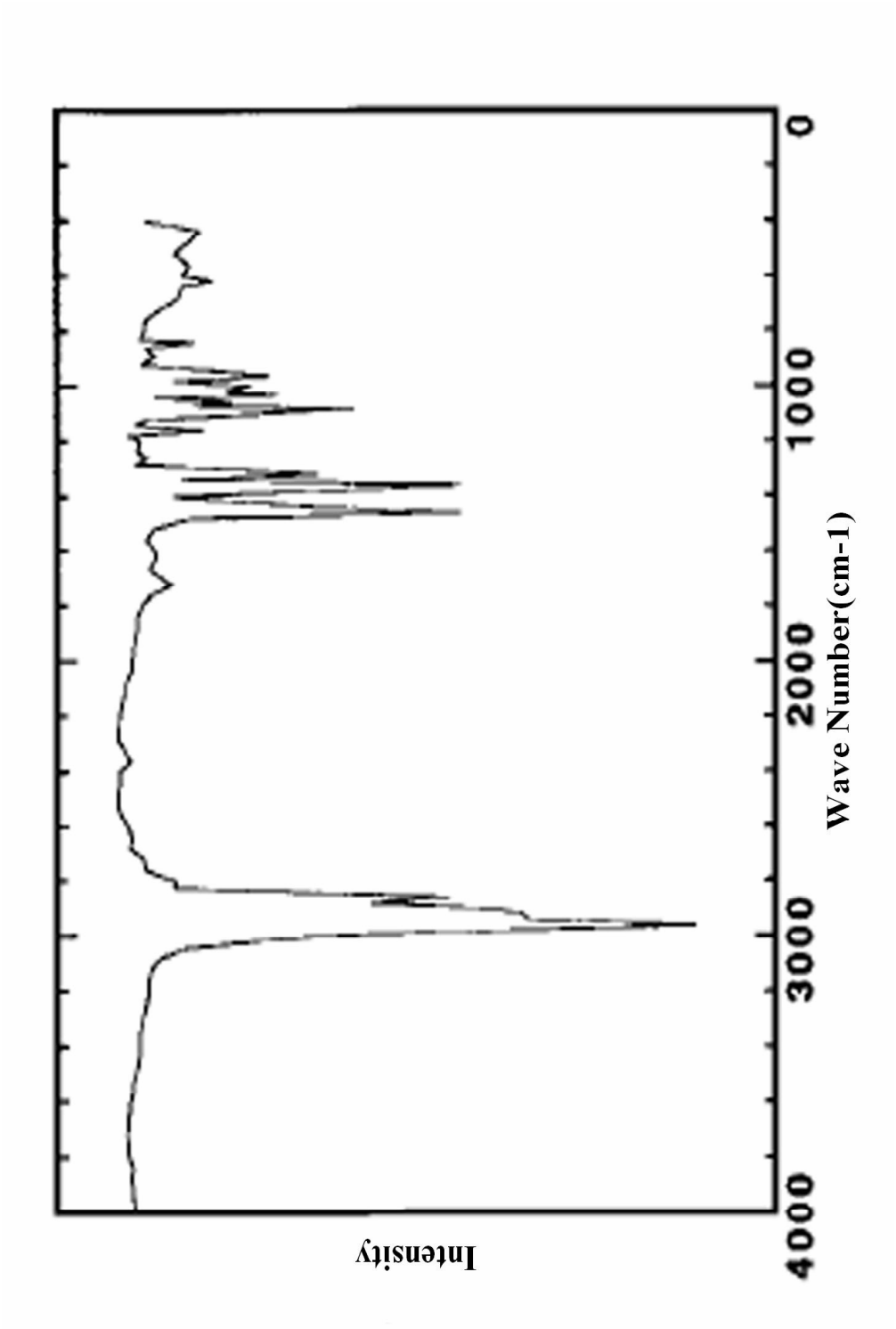

Figure 3.2 IR spectra of PMP (4000-400 cm^{-1})

bonded as well as non-bonded interactions, it is expected that the lower frequencies which also depend on the same set of non-bonded interaction would also be reasonably correct. A check can be provided by spectral observations in the far infrared region.

The normal mode frequencies are grouped into side chain modes, backbone modes and mixed modes (formed by coupling of backbone and side chain modes). The mixed modes show maximum dispersion and hence better elaborated under dispersion. The potential energy distribution and the matched observed frequencies along with calculated frequencies are given in Tables 3.2-3.4 at the zone centre and the zone boundary. Only those internal coordinates which have more than five percentage contribution in a particular mode are shown in the table.

3.3.1 Side chain modes

PMP consists of two chemical residue units in every structural repeat unit. The dominant feature of the side chain is the presence of gem-di-methyl group in one side and single methyl group on the other side of the backbone in each monomeric unit. The CH stretches of the methyl groups are highly localized and are generally observed in between 3000-2800 cm^{-1} in all the polymers having a methyl group. Since there are six methyl groups in the side chain, and in principle if they see different potential fields then each gives rise to slightly shifted asymmetric modes which are triply degenerate. These six triply degenerate asymmetric modes contribute to the width of the absorption line. These modes have been matched to the peak at 2960 cm^{-1}. Similarly the symmetric stretches are degenerate and fall within a narrow range (2859-2863 cm^{-1}) and assigned to reported peak at 2860 cm^{-1}. The peak at 1460 cm^{-1} has been assigned to the asymmetric degenerate deformation modes of the methyl groups which have been calculated in the range 1453-

1463 cm^{-1}. Six modes calculated in the range 1356-1368 cm^{-1} have contribution from symmetric deformation of the methyl group and matched with a broad peak at 1360 cm^{-1}.

The rocking modes depend upon the environment of the $–CH_3$ group. The modes calculated at 1004, 991, 981 cm^{-1} are assigned to observed value at 1001 cm^{-1} and modes at 959, 954 cm^{-1} assigned to observed peak at 960 cm^{-1} have major contribution from CH_3 rocking modes. Normal modes calculated at 921 and 922 cm^{-1} and assigned to 922 cm^{-1} in observed spectra have major contribution from single $–CH_3$ group rocking. Torsion modes for $–CH_3$ group found at very low value and calculated at 74, 74, 72 and 70 cm^{-1}.

3.3.2 Backbone modes

Backbone of PMP is chemically similar to polyacetylene [14], but differ in conjugation. In PMP two chemical repeat unit in a monomer are twisted at 90^o about C-C bond. The mode calculated at 1617 and 1612 and matched at 1615 cm^{-1} are predominant C=C stretch. This bond is very rigid in PMP in comparison to PA where this mode is assigned at 1470 cm^{-1}. C-C stretch is highly coupled. Modes calculated at 1133, 1028 cm^{-1} and assigned to peaks at 1120 and 1031 cm^{-1} respectively show significant contribution from C-C stretch. Due to rigidity, these modes are again obtained on higher side than in PA where they are obtained around 887 cm^{-1}.

3.3.3 Mixed Modes

The backbone and side chain attachment modes are known as mixed modes. These modes are highly coupled, generally dispersive in nature and belong to finger print region of the spectra of the molecule. The dispersive modes show an interesting property to bunch in pairs either towards the zone centre or at the zone boundary. Pair of modes calculated at

TABLE 3.2

Pure Side Chain mode and their assignments

Cal. freq.	Obs. freq.	Potential Energy Distribution (PED) at δ= 0.	Cal. freq.	Potential Energy Distribution (PED) at δ = π.
2960	2960	00)	2960	ν[C6-H](100)
2960	2960	ν[C6-H](100)	2960	ν[C6-H](100)
2960	2960	ν[C4-H](98)	2960	ν[C4-H](98)
2959	2960	ν[C4-H](99)	2959	ν[C4-H](99)
2959	2960	ν[C4-H](100)	2959	ν[C4-H](100)
2959	2960	ν[C4-H](100)	2959	ν[C4-H](100)
2921	2920	ν[C3-H](98)	2921	ν[C3-H](98)
2920	2920	ν[C3-H](98)	2920	ν[C3-H](98)
2863	2860	ν[C4-H](100)	2863	ν[C4-H](100)
2862	2860	ν[C4-H](100)	2862	ν[C4-H](100)
2862	2860	ν[C4-H](100)	2862	ν[C4-H](100)
2861	2860	ν[C6-H](100)	2861	ν[C6-H](100)
2861	2860	ν[C6-H](100)	2861	ν[C6-H](100)
2861	2860	ν[C4-H](100)	2861	ν[C4-H](100)
2859	2860	ν[C6-H](100)	2859	ν[C6-H](100)
2859	2860	ν[C4-H](100)	2859	ν[C4-H](100)
2859	2860	ν[C6-H](100)	2859	ν[C6-H](100)
2859	2860	ν[C4-H](100)	2859	ν[C4-H](100)
2859	2860	ν[C4-H](100)	2859	ν[C4-H](100)

2858	2860	ν[C4-H](100)	2858	ν[C4-H](100)
1464	1460	ϕ[H-C6-H](95)	1464	ϕ[H-C6-H](95)
1464	1460	ϕ[H-C6-H](95)	1464	ϕ[H-C6-H](95)
1462	1460	ϕ[H-C4-H](94)	1462	ϕ[H-C4-H](94)
1459	1460	ϕ[H-C4-H](94)	1459	ϕ[H-C4-H](94)
1458	1460	ϕ[H-C4-H](94)	1458	ϕ[H-C4-H](94)
1456	1460	ϕ[H-C4-H](92)	1456	ϕ[H-C4-H](92)
1456	1460	ϕ[H-C4-H](94)	1456	ϕ[H-C4-H](94)
1455	1460	ϕ[H-C4-H](88)+ϕ[C3-C4-H](6)+ϕ[H-C6-H](5)	1455	ϕ[H-C4-H](88)+ϕ[C3-C4-H](6)+ϕ[H-C6-H](5)
1454	1460	ϕ[H-C6-H](87)+ϕ[H-C4-H](8)	1454	ϕ[H-C6-H](86)+ϕ[H-C4-H](9)
1453	1460	ϕ[H-C4-H](90)	1453	ϕ[H-C4-H](89)+ϕ[H-C6-H](6)
1453	1460	ϕ[H-C6-H](74)+ϕ[H-C4-H](20)	1453	ϕ[H-C6-H](71)+ϕ[H-C4-H](24)
1453	1460	ϕ[H-C4-H](80)+ϕ[H-C6-H](15)	1453	ϕ[H-C4-H](77)+ϕ[H-C6-H](18)
1368	1360	ϕ[H-C4-H](49)+ϕ[C3-C4-H](45)	1368	ϕ[H-C4-H](49)+ϕ[C3-C4-H](45)
1366	1360	ϕ[H-C6-H](49)+ϕ[C1-C6-H](43)+ν[C1-C6](6)	1366	ϕ[H-C6-H](49)+ϕ[C1-C6-H](43)+ν[C1-C6](6)
1364	1360	ϕ[H-C4-H](49)+ϕ[C3-C4-H](45)	1364	ϕ[H-C4-H](49)+ϕ[C3-C4-H](45)
1362	1360	ϕ[H-C6-H](48)+ϕ[C1-C6-H](43)+ν[C1-C6](6)	1362	ϕ[H-C6-H](48)+ϕ[C1-C6-H](43)+ν[C1-C6](6)
1361	1360	ϕ[H-C4-H](48)+ϕ[C3-C4-H](45)	1361	ϕ[H-C4-H](48)+ϕ[C3-C4-H](45)
1356	1360	ϕ[H-C4-H](49)+ϕ[C3-C4-H](46)	1356	ϕ[H-C4-H](49)+ϕ[C3-C4-H](46)
1004	1001	ϕ[C3-C4-H](35)+ν[C1-C6](20)+ν[C3-C4](11)+ν[C2-C3](9)	1006	ϕ[C3-C4-H](27)+ν[C1-C6](24)+ν[C2-C3](9)+ ν[C3-C4](8)+ ν[C2-C17](6)+ϕ[C1-C6-H](5)
991	1001	ϕ[C3-C4-H](67)+ν[C3-C4](11)+ϕ[C4-C3-H](6)	986	ϕ[C3-C4-H](68)+ϕ[C1-C6-H](5)
981	1001	ϕ[C3-C4-H](67)+ν[C1-C6](7)	983	ϕ[C3-C4-H](66)+ϕ[C1-C6-H](6)
959	960	ϕ[C3-C4-H](38)+ν[C3-C4](30)+ϕ[C4-C3-H](18)+ ϕ[C2-C3-C4](6)	960	ϕ[C3-C4-H](37)+ν[C3-C4](28)+ϕ[C4-C3-H](18)+ϕ[C2-C3-C4](6)

954	960	ϕ[C3-C4-H](40)+ν[C3-C4](27)+ϕ[C4-C3-H](19)+ϕ[C2-C3-C4](5)	956	ϕ[C3-C4-H](38)+ν[C3-C4](25)+ϕ[C4-C3-H](19)+ϕ[C2-C3-C4](6)
922	922	ϕ[C1-C6-H](81)+ϕ[C3-C4-H](6)	925	ϕ[C1-C6-H](72)+ϕ[C3-C4-H](10)
921	922	ϕ[C1-C6-H](77)+ϕ[C3-C4-H](7)+ν[C1-C6](5)	924	ϕ[C1-C6-H](71)+ϕ[C3-C4-H](10)
900	892	ϕ[C1-C6-H](36)+ν[C1-C6](26)+ϕ[C3-C4-H](12)+ν[C2-C17](5)	900	ϕ[C1-C6-H](66)+ν[C1-C6](13)+ϕ[C3-C4-H](6)
898	892	ϕ[C1-C6-H](62)+ν[C1-C6](14)+ϕ[C3-C4-H](8)	899	ϕ[C1-C6-H](66)+ν[C1-C6](13)+ϕ[C3-C4-H](6)
891	892	ϕ[C3-C4-H](52)+ϕ[C1-C6-H](14)+ν[C2-C3](11)+ν[C2-C17](10)	887	ϕ[C3-C4-H](91)
887	892	ϕ[C3-C4-H](90)	883	ϕ[C3-C4-H](90)
883	892	ϕ[C3-C4-H](90)	872	ϕ[C3-C4-H](42)+ϕ[C1-C6-H](17)+ν[C2-C3](15)+ν[C1-C6](9)+ν[C2-C17](6)
843	840	ϕ[C3-C4-H](49)+ν[C3-C4](42)	843	ϕ[C3-C4-H](49)+ν[C3-C4](42)
839	840	ϕ[C3-C4-H](46)+ν[C3-C4](45)	839	ϕ[C3-C4-H](46)+ν[C3-C4](45)
755	-	ν[C3-C4](63)+ϕ[C3-C4-H](16)+ν[C1-C6](8)	757	ν[C3-C4](61)+ϕ[C3-C4-H](17)+ν[C1-C6](6)
74	-	τ[C3-C4](90)+τ[C17-C22](8)	76	τ[C3-C4](36)+τ[C17-C22](27)+ϕ[C1-C2-C17](9)+ϕ[C2-C17-C18] (8)+ϕ[C1-C2-C3](6)
74	-	τ[C3-C4](91)+τ[C17-C22](7)	74	τ[C3-C4](74)+τ[C17-C22](24)
72	-	τ[C3-C4](92)	73	τ[C3-C4](56)+τ[C17-C22](39)
70	-	τ[C3-C4](62)+ϕ[C3-C2-C17](12)+ϕ[C1-C2-C3](11)	72	τ[C3-C4](57)+τ[C17-C22](11)+ϕ[C1-C2-C17](10)+ϕ[C1-C2-C3](6)+ϕ[C2-C17-C18](6)

Note: All frequencies are in cm^{-1}.

TABLE 3.3

Backbone modes and their assignments

Cal. freq.	Obs. freq.	Potential Energy Distribution (PED) at δ = 0.	Cal. freq.	Potential Energy Distribution (PED) at δ = π.
1617	1615	ν[C1=C2](75)+ν[C2-C17](7)	1616	ν[C1=C2](77)
1612	1615	ν[C1=C2](80)	1615	ν[C1=C2](77)
1133	1120	ν[C2-C3](25)+ν[C2-C17](24)+ν[C1-C6](9)+ϕ[C1-C2-C17](7)+ϕ[C18-C17-C22](6)+ϕ[C3-C4-H](5)+ϕ[C1-C2-C3](5)+ϕ[C2-C17-C18](5)	1120	ν[C2-C3](28)+ν[C2-C17](23)+ν[C1-C6](9)+ϕ[C3-C4-H](7)+ϕ[C1-C2-C17](6) +ϕ[C18-C17-C22](5)+ϕ[C1-C2-C3](5)
1028	1031	ν[C1-C6](33)+ν[C2-C17](26)+ϕ[C1-C6-H](22)+ϕ[C18-C17-C22](7)	1008	ϕ[C3-C4-H](27)+ν[C1-C6](24)+ν[C3-C4](9)+ν[C2-C3](9) +ν[C2-C17](6)
621	621	τ[C17-C18](43)+ϕ[C2-C3-C4](9)+ν[C2-C3](8)+ν[C3-C4](7)	668	τ[C17-C18](23)+ν[C2-17](12)+ϕ[C1-C6-H](11)+ϕ[C2-C17-C22](8)+ϕ[C3-C2-C17](8)+ν[C3-C4](8)+ϕ[C1-C2-C17](6)
590	567	τ[C17-C18](45)+ϕ[C2-C3-C4](11)+ν[C3-C4](8)+ϕ[C2-C17-C22](8)+ν[C2-C3](7)+ϕ[C2-C17-C18](6)	563	ν[C2-C17](23)+τ[C17-C18](23)+ϕ[C2-C3-C4](11)+ν[C1-C6](9)+ν[C2-C3](9)+ν[C3-C4](5)
73	-	τ[C17-C22](86)+τ[C3-C4](11)	74	τ[C3-C4](80)+τ[C17-C22](18)
73	-	τ[C17-C22](85)+τ[C3-C4](13)	73	τ[C17-C22](51)+τ[C3-C4](37)
39	-	τ[C17-C18](23)+ν[C2-C17](20)+ϕ[C1-C2-C17](17)+τ[C2-C17](13)+ϕ[C1-C2-C3](6)	71	τ[C3-C4](29)+ϕ[C1-C2-C17](20)+ϕ[C2-C17-C18](12) +ϕ[C1-C2-C3](11)+τ[C17-C22](8)+ϕ[C18-C17-C22](7)+τ[C17-C18](7)
8	-	τ[C2-C17](79)+ν[C2-C17](6)	14	τ[C2-C17](81)+τ[C2-C3](7)
1	-	τ[C2-C17](85)+ϕ[C1-C2-C3](6)+ϕ[C3-C2-C17](6)	5	ϕ[C2-C17-C18](17)+ϕ[C2-C17-C22](16)+ϕ[C18-C17-C22](16)+ϕ[C1-C2-C17](15) +ϕ[C1-C2-C3](14)+ϕ[C3-C2-C17](14)

TABLE 3.4

Mixed modes and their assignments

Cal. freq.	Obs. freq.	Potential Energy Distribution (PED) at δ = 0.	Cal. freq.	Potential Energy Distribution (PED) at δ = π.
1321	1320	ϕ[C2-C3-H](55)+ϕ[C4-C3-H] (24)	1320	ϕ[C2-C3-H](55)+ϕ[C4-C3-H] (24)
1313	1320	ϕ[C2-C3-H](55)+ϕ[C4-C3-H] (23)	1313	ϕ[C2-C3-H](55)+ϕ[C4-C3-H] (23)
1164	1163	ϕ[C4-C3-H](68)+ν[C3-C4](19)+ϕ[C3-C4-H](7)	1164	ϕ[C4-C3-H](69)+ν[C3-C4](19)+ϕ[C3-C4-H](7)
1155	1163	ϕ[C4-C3-H](66)+ν[C3-C4](19)+ϕ[C3-C4-H](7)	1155	ϕ[C4-C3-H](68)+ν[C3-C4](19)+ϕ[C3-C4-H](7)
1084	1085	ν[C2-C3](42)+ϕ[C3-C4-H](19)+ν[C2-C17](10)+ϕ[C2-C3-H](5)	1120	ν[C2-C3](28)+ν[C2-C17](23)+ν[C1-C6](8)+ϕ[C3-C4-H](7)+ϕ[C1-C2-C17](6)+ϕ[C18-C17-C22](5)+ϕ[C1-C2-C3](5)
866	871	ϕ[C3-C4-H](38)+ϕ[C1-C6-H](23)+ν[C2-C3](16)+ν[C1-C6](10)	871	ϕ[C3-C4-H](43)+ϕ[C1-C6-H] (17)+ν[C2-C3](15)+ν[C1-C6](9)+ν[C2-C17](6)
792	792	ν[C3-C4](27)+ϕ[C1-C6-H](20)+ν[C2-C17](20)+ϕ[C3-C4-H](17)	763	ν[C3-C4](60)+ϕ[C3-C4-H](18)+ν[C1-C6](7)
727	720	ν[C3-C4](42)+ν[C2-C17](11)+ϕ[C1-C6-H](11)+ν[C1-C6](7)+ϕ[C3-C4-H](6)+ϕ[C1-C2-C17] (5)	670	τ[C17-C18](24)+ν[C2-C17](11)+ϕ[C1-C6-H](11)+ϕ[C2-C17-C22](8)+ν[C3-C4](8)+ϕ[C3-C2-C17](8)+ϕ[C1-C2-C17](5)
514	-	ϕ[C2-C3-C4](21)+ϕ[C2-C17-C22](15)+ϕ[C3-C2-C17](13) +ϕ[C4-C3-H](7)+ν[C2-C17](7)+ϕ[C18-C17-C22](7)+ ϕ[C1-C2-C17](6)	560	ν[C2-C17](24)+τ[C17-C18](22)+ϕ[C2-C3-C4](11)+ν[C1-C6](9)+ν[C2-C3](9)+ν[C3-C4](6)
451	445	ν[C1-C6](16)+ν[C2-C17](14)+ ϕ[C2-C17-C18](11)+ ν[C2-C3](10)+ϕ[C3-C2-C17](9)+ ϕ[C1-C2-C3](8)+τ[C17-C18](7)+ν[C3-C4](6)+ν[C1=C2](6)	438	ϕ[C2-C3-C4](15)+ϕ[C1-C2-C17](15)+ϕ[C2-C17-C18](12)+ ν[C2-C3](9)+ϕ[C1-C2-C3](6)+ϕ[C18-C17-C22](6)+ν[C2-C17](6)+ϕ[C3-C2-C17](5)
445	445	ϕ[C2-C3-C4](26)+ϕ[C1-C2-C17](16)+ϕ[C18-C17-C22](10)+ν[C2-C17](9)+ϕ[C2-C17-C22] (7)+ϕ[C4-C3-	435	ϕ[C2-C3-C4](14)+ϕ[C1-C2-C17](14)+ϕ[C2-C17-C18](13)+ ν[C2-C3](8)+ϕ[C1-C2-C3](6)+ϕ[C18-C17-

		H](6)+ν[C2-C3](6)		C22](6)+ϕ[C3-C2-C17](5)+ν[C2-C17](5)
389	-	ϕ[C2-C17-C18](13)+ν[C1-C6](12)+ϕ[C1-C2-C3](12)+ϕ[C4-C3-C5](11)+ϕ[C3-C2-C17](8)+ν[C3-C4](8)+ϕ[C4-C3-H](6)+ν[C2-C3](5)+ϕ[C18-C17-C22](5)	368	ϕ[C4-C3-C5](17)+ϕ[C4-C3-H](14)+ϕ[C2-C3-C4](8)+ϕ[C1-C2-C3](8)+ν[C3-C4](7)+ν[C2-C17](7)+ϕ[C3-C2-C17](7)+ϕ[C2-C3-H](5)
333	-	ϕ[C4-C3-C5](35)+ϕ[C4-C3-H](15)+ϕ[C2-C3-C4](10)+ϕ[C2-C3-H](5)+ϕ[C2-C17-C22](5)	368	ϕ[C4-C3-C5](17)+ϕ[C4-C3-H](14)+ϕ[C2-C3-C4](8)+ϕ[C1-C2-C3](8)+ν[C3-C4](7)+ν[C2-C17](7)+ϕ[C3-C2-C17](7)+ϕ[C2-C3-H](5)
319	-	ϕ[C4-C3-C5](24)+ϕ[C2-C17-C18](15)+ϕ[C4-C3-H](12)+τ[C17-C18](11)+ϕ[C2-C3-C4] (9)+ϕ[C2-C17-C22](7)	303	ϕ[C2-C3-C4](29)+ϕ[C2-C17-C22](17)+ϕ[C18-C17-C22](13)+ϕ[C4-C3-C5](11)+τ[C17-C18](9)
271	-	ϕ[C2-C3-C4](51)+ϕ[C4-C3-C5](19)+ϕ[C2-C17-C22](9)+ϕ[C1-C2-C17](5)	301	ϕ[C2-C3-C4](29)+ϕ[C2-C17-C22](17)+ϕ[C18-C17-C22](13)+ϕ[C4-C3-C5](13)+τ[C17-C18](8)
266	-	ϕ[C2-C3-C4](51)+ϕ[C4-C3-C5](26)	272	ϕ[C4-C3-C5](35)+ϕ[C2-C3-C4](30)+ϕ[C2-C17-C18](9)
234	-	ϕ[C2-C3-C4](27)+ϕ[C18-C17-C22](22)+ϕ[C2-C17-C22](18)+ϕ[C4-C3-C5](16)+ν[C2-C3](6)	271	ϕ[C4-C3-C5](35)+ϕ[C2-C3-C4](31)+ϕ[C2-C17-C18](9)
219	-	ϕ[C2-C3-C4](31)+ϕ[C2-C17-C22](28)+ϕ[C18-C17-C22](14)+ϕ[C4-C3-C5](12)+ν[C2-C3](6)	215	ϕ[C2-C3-C4](32)+ϕ[C2-C17-C22](28)+ϕ[C18-C17-C22](14)+ϕ[C4-C3-C5](9)
154	-	ϕ[C2-C17-C18](21)+ϕ[C2-C3-C4](20)+ϕ[C18-C17-C22](19)+ϕ[C1-C2-C17](15)+ϕ[C1-C2-C3](8)	215	ϕ[C2-C3-C4](32)+ϕ[C2-C17-C22](28)+ϕ[C18-C17-C22](14)+ϕ[C4-C3-C5](9)
132	-	ϕ[C1-C2-C17](32)+ϕ[C18-C17-C22](18)+ ϕ[C2-C3-C4](14)+τ[C17-C18](11)+ϕ[C2-C17-C18](7)+ϕ[C1-C2-C3](6)	121	ϕ[C3-C2-C17](31)+ϕ[C2-C3-C4](18)+ϕ[C1-C2-C3](17)+τ[C17-C18](7)+ϕ[C4-C3-H](7)
108	-	ϕ[C1-C2-C3](28)+ϕ[C3-C2-C17] (26)+τ[C17-C18](7)+ϕ[C2-C3-C4](7)+ϕ[C4-C3-H](6)+ν[C2-C17](6)+ϕ[C2-C17-C22](5)	121	ϕ[C3-C2-C17](31)+ϕ[C2-C3-C4] (19)+ϕ[C1-C2-C3](16)+τ[C17-C18](8)+ϕ[C4-C3-H](6)
78	-	τ[C3-C4](32)+ϕ[C3-C2-C17] (21)+ϕ[C1-C2-C3](16)+ϕ[C2-C17-C18](6)	76	τ[C3-C4](22)+ϕ[C1-C2-C17](17)+τ[C17-C22](15)+ϕ[C2-C17-C18](13)+ϕ[C1-C2-C3](11)+τ[C17-C18](8)+ϕ[C18-C17-C22](7)
26	-	τ[C2-C3](93)	29	τ[C2-C3](84)+τ[C17-C18](7)+τ[C2-C17](5)

25	-	τ[C2-C3](93)	28	τ[C2-C3](84)+τ[C17-C18](7)+τ[C2-C17](5)
6	-	ϕ[C2-C17-C18](37)+ϕ[C18-C17-C22](28)+ϕ[C2-C17-C22](28)	13	τ[C2-C17](84)+τ[C2-C3](8)
4	-	ϕ[C2-C17-C18](37)+ϕ[C18-C17-C22](30)+ϕ[C2-C17-C22](29)	6	ϕ[C2-C17-C18](22)+ϕ[C2-C17-C22](21)+ ϕ[C18-C17-C22](20)+ϕ[C1-C2-C17](9)+ϕ[C1-C2-C3](9)+ϕ[C3-C2-C17](8)+τ[C2-C17](5)
0	-	ϕ[C3-C4-H](50)+ϕ[H-C4-H](45)	4	ϕ[C1-C2-C3](22)+ϕ[C3-C2-C17](21)+ϕ[C1-C2-C17](19)+ ϕ[C2-C17-C18](12)+ϕ[C18-C17-C22](11)+ϕ[C2-C17-C22](10)
0	-	ϕ[C3-C4-H](50)+ϕ[H-C4-H](45)	3	ϕ[C1-C2-C3](19)+ϕ[C3-C2-C17](19)+ϕ[C1-C2-C17](17)+ ϕ[C2-C17-C18](14)+ϕ[C18-C17-C22](13)+ϕ[C2-C17-C22](13)

Note: All frequencies are in cm^{-1}.

154 and 219 cm^{-1}, having major contributions from C-C-C and C-C=C bending vibrations, show unique behavior. Upper mode is almost non-dispersive, but lower mode show large dispersion of 61 cm^{-1}. Both modes bunch at zone boundary.

3.4 Dispersion curves

Other than providing knowledge of the density of states, the profile of the dispersion curves gives information on the extent of interaction of mode along the chain. Modes above 1150 cm^{-1} are non-dispersive in nature. Therefore, dispersion curves are plotted below 1150 cm^{-1} and are shown in Figs. 3.3(a) and 3.4(a). Characteristic feature of dispersion curves like crossing over of modes, repulsion and von Hoe type singularity arise due to internal symmetry. Pair of modes at (108 and 132 cm^{-1}), (271 and 319 cm^{-1}) and (445 and 451 cm^{-1}) show repulsion and exchange of character at $\delta = 0.293\pi$, 0.55π and 0.123π respectively. This repulsion and exchange of phonon characters is analogous to the collision of two identical particles moving in opposite directions in classical mechanics. They exchange their momentum after collision.

Mode calculated at 108 cm^{-1} having major contributions from the angle bends [C1-C2-C3], [C3-C2-C17] and [C17-C18] torsion starts dispersion at $\delta=0.15\pi$ and come close to mode at 132 cm^{-1} with dominant contributions from [C1-C2-C17], [C18-C17-C22] and [C2-C3-C4] angle bends and [C17-C18] torsion. At $\delta=0.25\pi$ their PEDs start mixing and they exchange character and repel at $\delta=0.293\pi$. On increasing δ, the lower mode become almost non-dispersive. The other mode bunches with this at zone boundary.

Pair of modes at 271 & 319 cm^{-1} comes close and then diverge. In the first mode contribution of [C2-C3-C4] bend decreases while contribution from [C1-C2-C17] and [C18-C17-C22] bends increase. Other mode show increasing contribution of [C2-C3-C4] bend and decreasing contributions from [C2-C17-C18] and [C4-C3-H] bends

till $\delta=0.55\pi$. At this δ value they exchange their PEDs and repel each other. After repulsion these modes again bunch at zone boundary and their PEDs become equal.

The mode calculated at 445 cm^{-1} having contributions from [C2-C3-C4], [C1-C2-C17], [C18-C17- C22] bendings and [C2-C17] stretch, starts mixing near zone center at $\delta=0.08\pi$ and exchanges its PED at $\delta=0.123\pi$ with the neighboring mode calculated at 451 cm^{-1} having contributions from [C1-C6], [C2-C17], [C2-C3], [C1=C2] stretches and [C2-C17-C18], [C3-C2-C17], [C1-C2-C3] bendings and [C17-C18] torsion. As δ is increased these modes show large dispersion and have maximum separation of 58 cm^{-1} at $\delta=0.70\pi$. Beyond $\delta=0.75\pi$ they further come close and bunch at zone boundary.

3.3.5 Frequency distribution function and heat capacity

The frequency distribution obtained from the dispersion curves for the isolated chain of PMP is plotted in Figs. 3.3(b) and 3.4(b). The peaks in the frequency distribution curves corresponding to the regions of high density-of-states compare well with the observed frequencies. The frequency distribution function is further used in calculating the heat capacity of PMP. The predictive values of heat capacity are plotted against temperature in Fig. 3.5. Modes which are purely side chain, purely backbone and a mixture of two are given in Tables 3.2, 3.3 and 3.4 respectively. Their contributions to the heat capacity have also been calculated separately and plotted in Fig. 3.5.

The maximum contribution comes from the mixed modes. The data are given in the temperature range 10-450 K. The contribution from the lattice modes should have appreciable effect on the heat capacity because of its sensitivity to these modes.

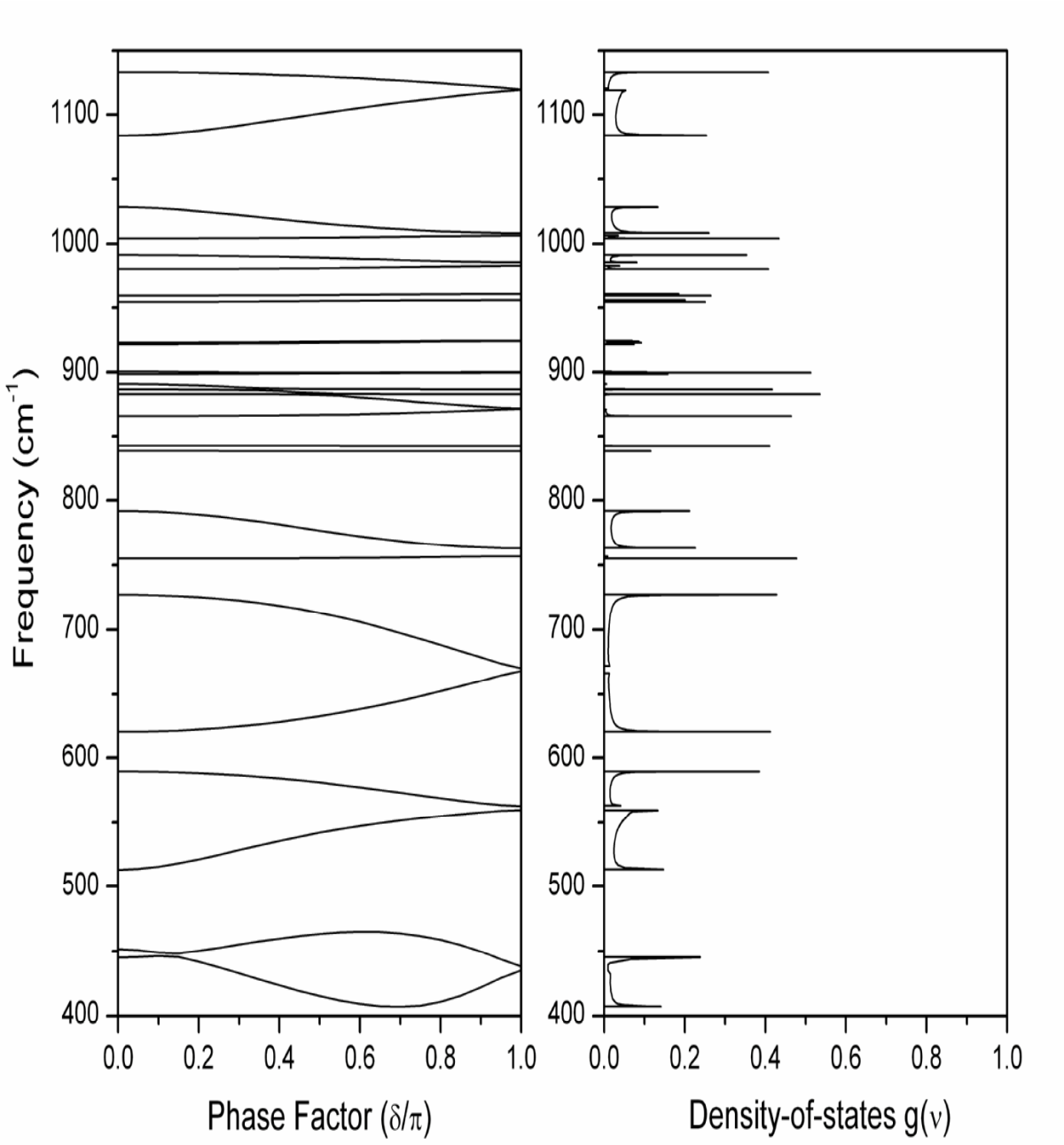

Figure 3.3(a) **Figure 3.3(b)**

Figure 3.3 (a) Dispersion curves; and (b) Density-of-states function of PMP in frequency range 1150-400 cm^{-1}

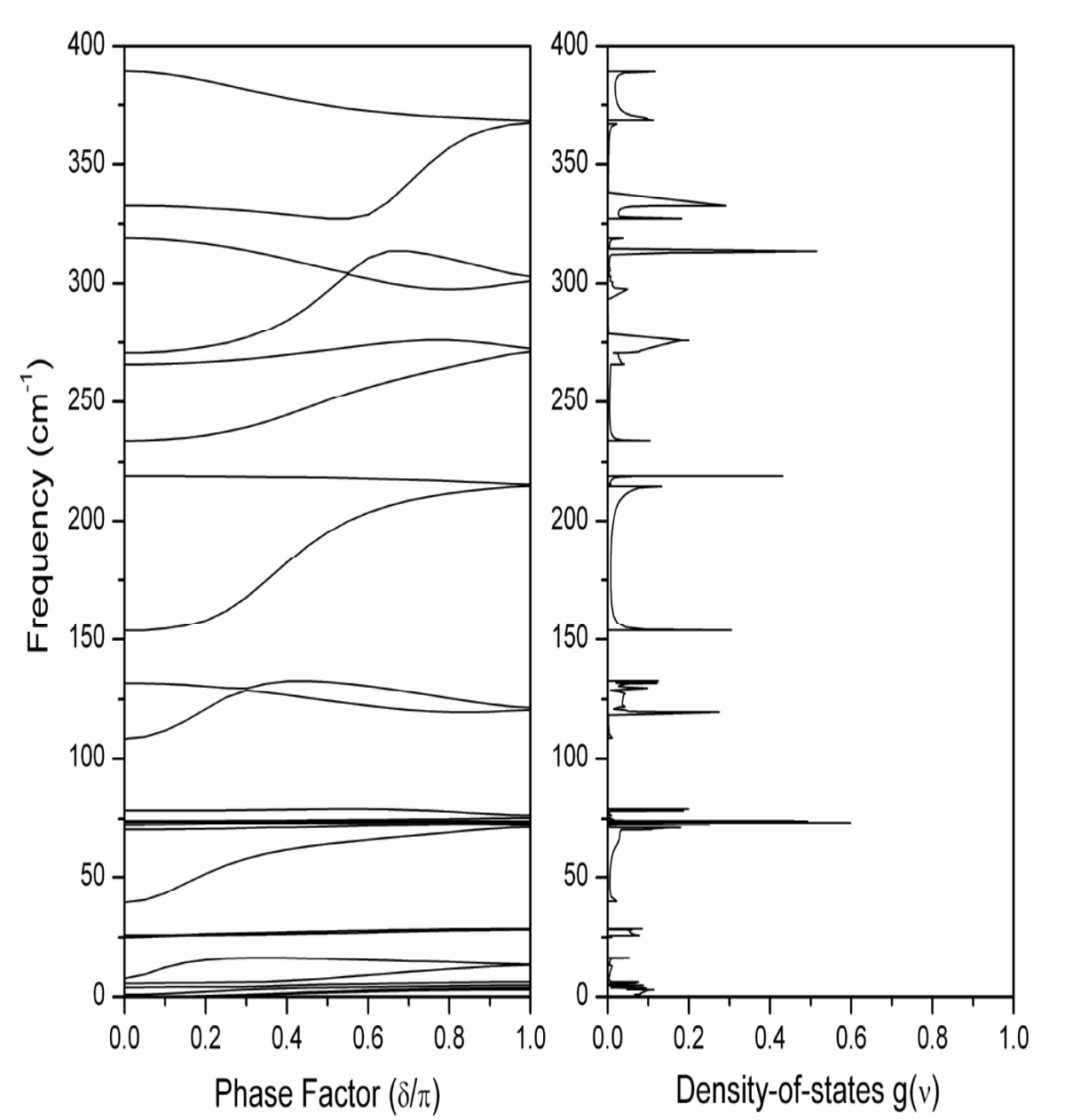

Figure 3.4(a) **Figure 3.4(b)**

Figure 3.4 (a) Dispersion curves; and (b) Density-of-states function of PMP below 400 cm^{-1}

The calculations of dispersion curves for a three-dimensional crystal is extremely difficult because of the large size of the dynamical matrix and enormous number of interactions. Thus, in spite of several limitations involved in the calculation of heat capacity and absence of experimental data, the present work does provide a good starting point for further basic studies on the thermodynamical behaviour of PMP.

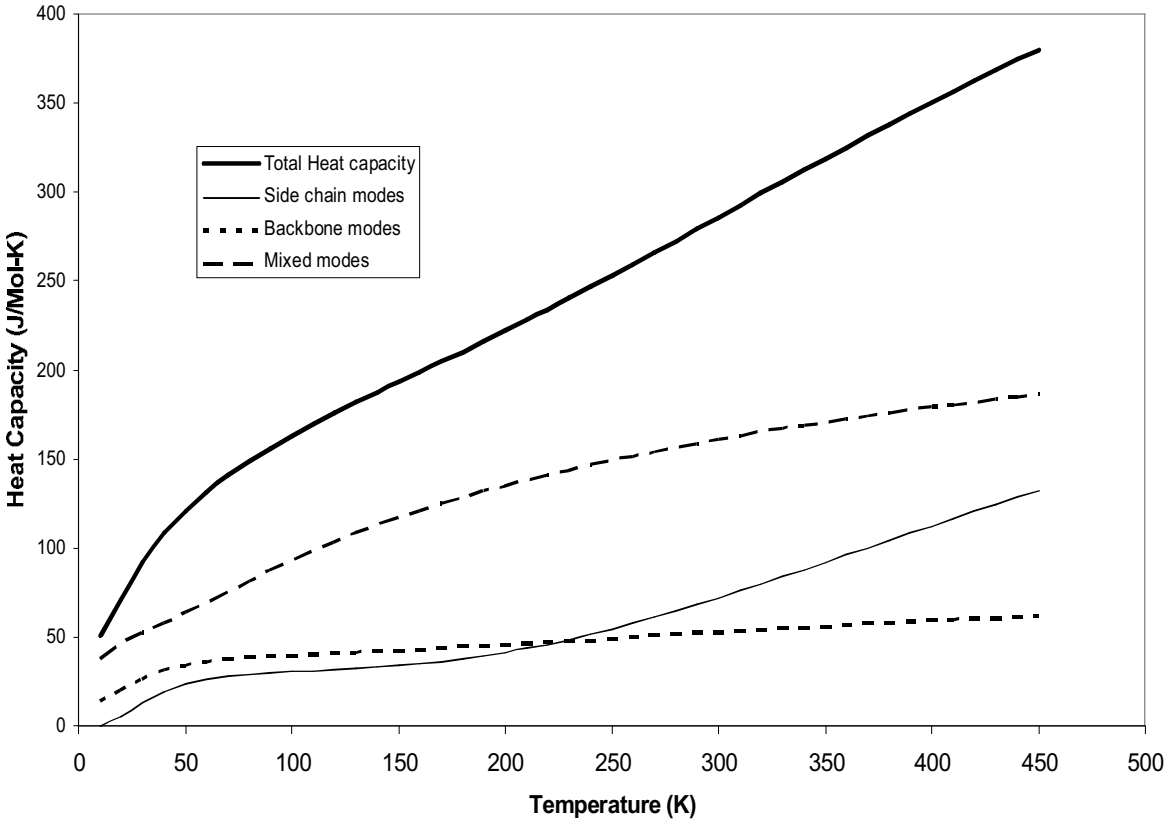

Figure 3.5 Variation of Heat capacity C_v with temperature (10-450K)

CONCLUSION

This chapter provides a better understanding of the poly(4-methyl-2-pentyne) spectra by assigning bands based on Potential energy distribution. The spectral data of the PMP can be successfully interpreted from the vibrational dynamics based on all the characteristic features of dispersion curves, such as regions of high density-of-states, repulsion and convergence/divergence of modes near zone centre/boundary. In addition, the heat capacity as a function of temperature in the region 10-450 K has been calculated.

REFERENCES

[1] J. C. W. Chien, "*Polyacetylene*", Academic Press, New York, (1984).

[2] J. W. Y. Lam, B. Z. Tang, *Acc. Chem. Res.*, 38 (2005) 745.

[3] I. Pinnau, L.G. Toy, *J. Membrane Sci.*, 116 (1996) 199.

[4] Z. He, I. Pinnau, A. Marisato, *Desalination*, 146 (2002) 11.

[5] I. Pinnau, Z. He, *US Patent*, 6316 (2001) 684.

[6] A Morisato, I. Pinnau, *J. Membr. Sci.*, 121 (1996) 243.

[7] T. C. Merckel, B. D. Freeman, R.J. Spontak, Z. He, I. Pinnau, P. Meakin, A. J. Hill, *Science*, 296 (2002) 519.

[8] H. Izumikawa, T. Masuda, T. Higashimura, *Polym. Bull.*, 27 (1991) 193.

[9] V. S. Khotimsky, S. M. Matson, E. G. Litvinova,G. N. Bondarenko, A. I. Rebrov, *Polym. Sci., Ser. A*, 45 (8) (2003) 740.

[10] A. Morisato, I. Pinnau, *J. Membrane Sci.*, 121 (1996) 243.

[11] P. W. Higgs, *Proc. Roy. Soc. London A*, 220 (1953) 472.

[12] E. B. Wilson Jr., J. C. Decius, P. C. Cross, "*Molecular vibrations: The theory of Infrared and Raman Vibrational Spectra*", Dover Publications New York (1980).

[13] H. C. Urey, C. A. Bradley, *Phys. Rev.*, 38 (1931) 1969.

[14] A. Kumar, S. Pande, P. Tandon, V. D. Gupta, *J. Macromol. Sci. Part B*, 39 (3) (2000) 303.

[15] S. Pande, A Kumar, P. Tandon, V. D. Gupta, *Vib. Spectrosc.*, 805 (2001) 1.